ARTICLES

Journal of Semiconductors
(2022) 43, 022101
doi: 10.1088/1674-4926/43/2/022101

Defects properties and vacancy diffusion in Cu_2MgSnS_4

Kin Fai Tse, Shengyuan Wang, Man Hoi Wong, and Junyi Zhu†

Department of Physics, The Chinese University of Hong Kong, Hong Kong, China

Abstract: Cu_2ZnSnS_4 (CZTS) is a promising photovoltaic absorber material, however, efficiency is largely hindered by potential fluctuation and a band tailing problem due to the abundance of defect complexes and low formation energy of an intrinsic Cu_{Zn} defect. Alternatives to CZTS by group I, II, or IV element replacement to circumvent this challenge has grown research interest. In this work, using a hybrid (HSE06) functional, we demonstrated the qualitative similarity of defect thermodynamics and electronic properties in Cu_2MgSnS_4 (CMTS) to CZTS. We show Sn_{Mg} to be abundant when in Sn- and Cu-rich condition, which can be detrimental, while defect properties are largely similar to CZTS in Sn- and Cu-poor. Under Sn- and Cu-poor chemical potential, there is a general increase in formation energy in most defects except Sn_{Mg}, Cu_{Mg} remains as the main contribution to p-type carriers, and Sn_{Mg} may be detrimental because of a deep defect level in the mid gap and the possibility of forming defect complex Sn_{Mg}+Mg_{Sn}. Vacancy diffusion is studied using generalized gradient approximation, and we find similar vacancy diffusion properties for Cu vacancy and lower diffusion barrier for Mg vacancy, which may reduce possible Cu-Mg disorder in CMTS. These findings further confirm the feasibility of CMTS as an alternative absorber material to CZTS and suggest the possibility for tuning defect properties of CZTS, which is crucial for high photovoltaic performance.

Key words: CMTS; CZTS; defect; hybrid functional; diffusion

Citation: K F Tse, S Y Wang, M H Wong, and J Y Zhu, Defects properties and vacancy diffusion in Cu_2MgSnS_4 [J]. *J. Semicond.*, 2022, 43(2), 022101. http://doi.org/10.1088/1674-4926/43/2/022101

1. Introduction

Kesterite Cu_2ZnSnS_4 (CZTS) is an earth-abundant, non-toxic absorber material for photovoltaics with a direct band gap tunable from 1.5 eV in pure CZTS[1–3] to 1.0 eV in pure $Cu_2ZnSnSe_4$[1, 4] by anion mixing of S and Se and a high band edge absorption coefficient larger than 10^4 cm^{-1}[4]. The record efficiency of alloyed $CZTS_xSe_{1-x}$ (CZTSSe) is at 12.6%[5] using solution process, and a 11% efficient pure CZTS absorber device is recently achieved[6].

Comparing CZTS to the $Cu(In/Ga)S_2$ (CIGS) absorber material, CZTS often suffers from a high open-circuit voltage (V_{OC}) deficit[7–9] larger than 0.6 eV, low external quantum efficiency (EQE) in the long wavelength region, low carrier lifetime, and thus fill factor[10]. These observations are commonly attributed to the abundance of point defects and defect complexes[11, 12], band edge or electrostatic potential fluctuation induced by defect compensation[13], interface defects[14, 15], unfavorable band alignment[16, 17] and secondary phases due to composition inhomogeneity, and back contact decomposition[15, 18]. Defect abundance in CZTS originates from the intrinsically low formation energy of point defects in thermodynamic limit[8, 19]. Moreover, the formation of defect complexes and clusters, such as Cu_{Zn}+Zn_{Cu}, is favored energetically and entropically[20, 21], resulting in a transition to Cu–Zn disordered kesterite at a low temperature of 200–260 °C[22]. The high density of defects in disordered kesterite may introduce a defect band within the band gap[8] that contributes to band tailing and electrostatic potential fluctuation[15]. Additionally, CZTS shows strong Cu/Zn compositional fluctuation due to low lattice mismatch to secondary phases[23, 24]. Also a back-contact decomposition reaction is suggested to be responsible for secondary phases segregation near the back contact[25, 26]. These challenges of CZTS were extensively studied in literature and various processing strategies were proposed to mitigate the problems, including annealing at low-temperature[8] and high sulphurization pressure[25, 27], surface etching[25, 28], interface passivations[29–31], alternative buffer layers[32–35] and back-contact passivations[26, 36–40].

Despite the theoretical and experimental efforts in the development of processing techniques, an empirically lower EQE and V_{OC} still persists in CZTSSe, contributing to the efficiency gap compared to record efficiency of higher than 20% in other thin film materials such as CIGS. It is suggested that intrinsic phase stability and electronic properties play an important role in the construction of high efficiency kesterite solar cells[15, 16]. Element substitution or alloying starting from CZTS can provide a large number of candidate material alternatives with similar but modified structural and electronic properties[41, 42]. It is thus a promising strategy for tuning defect properties in CZTS. Since the band edge positions of CZTS are determined by Cu-d/S-p and Sn-s/S-p hybridization at the valence band (VB) and conduction band (CB) respectively[1], band alignment and defect properties are mainly determined by the choice of group I, IV, VI elements. A large portion of the phase diagram in CZTS is governed by the phase boundary due to decomposition reaction into ZnS and Cu_2SnS_3[41]. As a result, the phase stability of CZTS may be tuned independently by the substitution of group II elements. A number of element substitutions were investigated in detail from theoretical or experimental approaches. Anion S/Se mixing is used to adjust the band edge position and band gap[16]. Ag_2ZnSnS_4

Correspondence to: J Y Zhu, jyzhu@phy.cuhk.edu.hk
Received 8 JULY 2021; Revised 29 JULY 2021.

suppresses p-type defect and widen the band gap due to low VB and become weakly n-type[43], and Ag composition grading is proposed to reduce Fermi level pinning[43, 44]. Up to 40% Cd substitution to Zn is found to be beneficial to device performance attributed to the reduction of ZnS phase[45], and 40%–50% of Ge substitution can reduce V_{OC} deficit and increase the bandgap by up to 0.3 eV[46, 47].

Cu_2MgSnS_4 (CMTS) is also a viable alternative that is less investigated in literature. Early work based on semi-local exchange-correlational functional predicts CMTS to have a small instability with respect to phase segregation into Cu_2SnS_4 and MgS[41]. However, later experiments had reported successful synthesis of CMTS[48–50], which contradict early conclusions. Agawane *et al.* synthesized $Cu_2Zn_xMg_{1-x}SnS_4$ by pulsed laser deposition covering $x = 0$ to $x = 1$, showing an increasing band gap with a fraction of Mg substitution and improved grain morphology at 50% Zn replaced with Mg[49]. Existence of CMTS phase is confirmed by x-ray diffraction and Raman spectroscopy for pure Mg sample without addition of Zn[49]. Improved carrier mobility and reduced secondary phases is reported by an Mg/Zn alloying strategy[51, 52]. A device using a pure CMTS absorber layer with 0.78% efficiency was fabricated only recently[50].

CMTS is different from CZTS in that 1) a more ionic and larger covalent radius Mg replaces the role of Zn in CZTS; 2) the competing secondary phase MgS is of halite structure instead of the zinc-blende structure; and 3) the ground-state structure of CMTS is stannite, where Cu and Sn/Zn ions are organized into layers[42]. These differences may lead to major consequences in the phase diagram, type and concentration of ionizable defects and deep traps, and diffusion kinetics of defects. Understanding CMTS differences and similarities compared to CZTS can guide important design choices in the fabrication process. Although a large body of literature is available from first-principles calculations and experiments for CZTS, to our knowledge, only a handful of experiment studies are available[48–52], and theoretical studies are largely absent for CMTS. We investigate the defect thermodynamics, electronic properties and defect diffusion kinetics of CMTS, and provide a direct comparison with CZTS[11, 12]. Our result shows that CMTS shares a significant similarity in major carrier providers (Cu_{Mg}), a lower diffusion barrier for Mg, and a reduction in defect density and detrimental defects, which can be beneficial to device performance. We identified a change in dominant detrimental defect in CMTS to Sn_{Mg} related defects. We also examined favorable thermodynamic conditions and strategies to control this Sn-related defect based on our first-principles results.

2. Electronic and thermodynamic properties

The phase diagram is calculated following the methodology of our earlier study for ease of discussion. The atomic chemical potential corresponding to the growth window of CMTS is calculated by requiring that, under the chemical potential window specified, CMTS is energetically stable while other secondary phases are unstable. Detailed thermodynamic discussions of CMTS are referred to in Ref. [42]. Formation energies for binary secondary phases including halite and zinc-blende MgS, and ternary secondary phases in CMTS as listed in other related works[11, 53] are calculated with reference

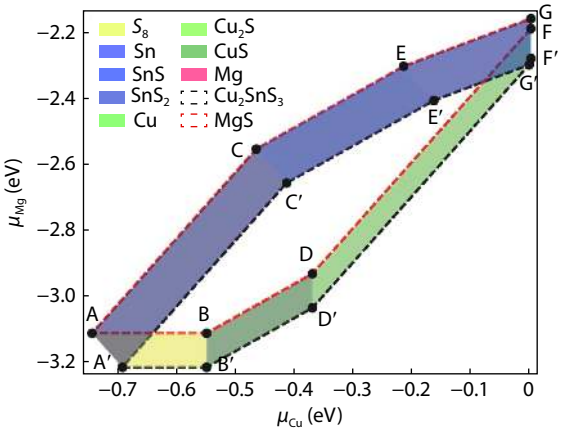

Fig. 1. (Color online) Phase diagram of CMTS calculated from hybrid functional (HSE06).

to element fcc-Cu, hcp-Mg, grey Sn and S_8 phases. In the CMTS phase, a sizable growth window exists when calculated under a hybrid functional, indicated by the colored region of Fig. 1. The range of zero-temperature chemical potentials, at which CMTS is energetically more stable than secondary phases, are used as an estimation to the range of free energy at which CMTS can be formed spontaneously. The shape of the CMTS phase diagram resembles that of CZTS, and the growth window is largely limited by the relative stability between CMTS and MgS and Cu_2SnS_3 phases. Cu poor chemical potential is in general S richer within the growth window, indicating that a higher sulphur pressure is thus preferred for CMTS growth under Cu deficit.

We calculated a direct band gap of 1.61 eV for CMTS, showing a hybridization of Cu-3d (Sn-5s) and S-3p orbitals that are composed of the VB (CB). Meanwhile, Mg is not involved in the composition of VB or CB. Band alignment of CMTS with reference to CZTS is calculated through a CMTS(010)/CZTS(010) hetero-junction following the methodology of Himuma *et al.*[54]. The increase in band gap is almost entirely due to a higher CB by +198 meV.

3. Intrinsic defect formation

The formation of defect is governed by both the growth condition (atomic chemical potential) and the Fermi energy level, at equilibrium, the formation energy ΔH of a defect D with charge q can be expressed as[55–57]

$$\Delta H(D,q) = [E(D,q) - E_0] + E_{\rm corr}(D,q) + \sum_i [n_i(E_i + \mu_i)] + q(\varepsilon_{\rm VBM} + E_{\rm F}), \quad (1)$$

where the third term sums over the energy required to remove n_i (negative for add) atom of species i to corresponding element reservoir, and the last term accounts for the energy required to remove q electrons to an electron reservoir equivalent to the host cell. $E_{\rm corr}$ represents the Freysoldt–Neugebauer–Van de Walle (FNV) finite-size correction[56]. First-principles simulation using Heyd–Scuseria–Ernzerhof (HSE06) hybrid functional is performed by a periodic supercell containing 64 atoms per defective atom, for 64 atom supercell, a Γ-centered 2 × 2 × 2 is chosen and a 600 eV plane-wave cut-off is used. The accuracy in defect calculation is set to 10^{-4} eV/atom, while ionic relaxation will stop when the

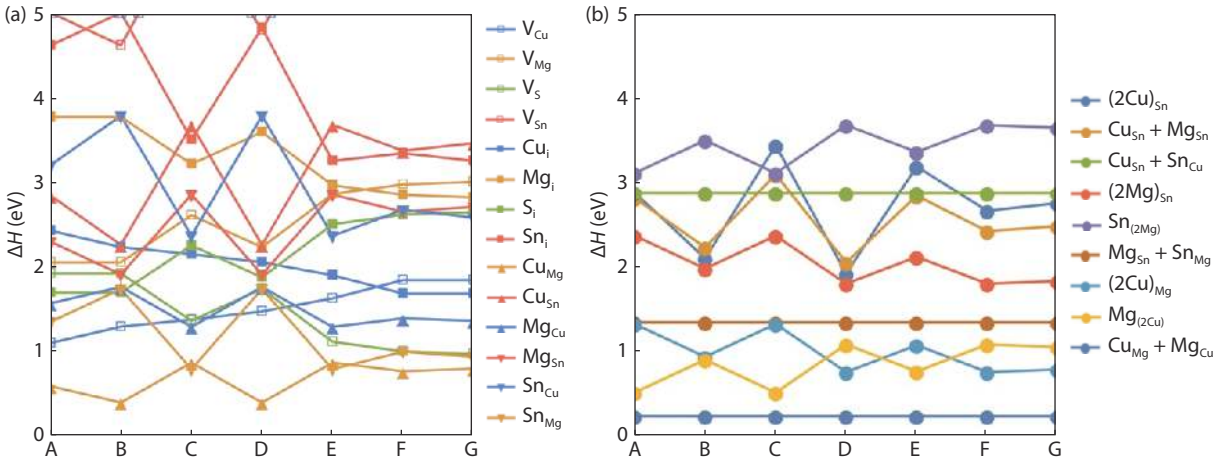

Fig. 2. (Color online) Neutral defect formation energy for (a) intrinsic defects and (b) defect complexes in CMTS at chemical potentials ranging from Cu poorest (A) to Cu richest (G).

forces reach 10^{-2} eV/Å. During relaxation with a hybrid functional, Fock exchange potential is evaluated on a reduced k-grid by a factor of 2, such reduction is tested to recover accurate defect structure while mitigating the stiff computational requirement of the hybrid functional. The detailed convergence tests are available in the supplementary information. We first discuss the effect of growth condition on defect populations in CMTS. The neutral defect formation energy of intrinsic defects in stannite CMTS are shown in Fig. 2, and only the lowest energy of symmetrically distinct configurations is reported.

The local bonding environment of CMTS largely follows that of CZTS, in which one S atom is bonded directly to 2 Cu, 1 group II and 1 Sn atom, and each cation is bonded to 4 S atoms. We therefore expect that defect properties will be somewhat similar to CZTS. On the other hand, the difference in electronic structure and local stress can also enhance or suppress defect formation selectively where a larger size difference leads to an increase in defect formation energy[58, 59]. In the literature of CZTS, defects with formation energy below 1.5–2.0 eV[11], which will be highlighted below, are considered to have a concentration high enough to modify device performance. The formation energy of Cu_{Mg} is lower than 1.0 eV at all chemical potential similar to CZTS, indicating a relatively high concentration of Cu_{Mg} that can be formed under most growth conditions. V_{Cu} has a formation energy of 1.10 eV in the Cu poorest limit, and the formation energy increases as μ_{Cu} increases. Sn_{Mg} has a lower neutral defect formation energy compared to Sn_{Zn} in CZTS, which can be explained by the lower donor level that is fully occupied. The neutral defect formation energies from point A' to G' are qualitatively similar to point A to G, with only minor shift in formation energy due to slight difference in the choice of chemical potential.

Several defects including Cu_i, Mg_{Cu}, Sn_{Mg} and V_S have lower formation energy in Cu rich limit (points E, F and G), while the formation energy of acceptor defects V_{Cu} and Cu_{Mg} becomes higher. As a result, the Cu rich condition may lead to stronger charge compensation and higher concentration of donor defects that may deteriorate device performance. At chemical potential point B and D, neutral formation energy of all point defects except Cu_{Mg} and V_{Cu} is above 1.6 eV. These chemical potentials correspond to a mildly Cu poor and Sn poor growth condition. As a comparison, the formation energy of a number of donor defects in CZTS are always between 1–1.5 eV at any chemical potential[11, 12]. There is also a general increase in defect formation energy for all point defects calculated except Sn_{Mg}. From a quasi-chemical model, the concentration of defect D can be related to its free energy by

$$[D] = N_i g e^{-\Delta H_f / k_b T}, \quad (2)$$

where N_i is the density of site (Cu = 1.2×10^{22}, Mg/Sn = 6.0×10^{21}, S = 2.4×10^{22} cm^{-3} in CMTS) and g account for structural and electronic degeneracy. A higher defect formation energy for deep defect can help reduce detrimental defect density. Thus by fine tuning the metallic precursor ratio[34, 60] towards Cu and Sn poor, the density of most defects can be reduced. Moreover, if defects in CMTS equilibrate at a lower temperature of 400 °C instead of 550 °C, the Boltzmann factor in Eq. (2) with ΔH_f = 1.6 eV can be further reduced by more than two orders of magnitude, suggesting that careful the control of temperature profile or the annealing of CMTS film at a lower temperature may help reduce bulk defect density. These growth strategies can be beneficial to carrier lifetime.

4. Defect complexes

Defect complexes can have significant influence on band edge positions[12], so that device performance can be affected if some defect complex can potentially exist in abundance. The binding energy (E_{bind}) of a defect complex is defined as the energy gained by forming defect complex from separated point defects[53], i.e., $E_{bind} = \Delta H_{\alpha\beta} - \Delta H_\alpha - \Delta H_\beta$. The binding energy is independent of chemical potential as it reflects only the energy difference between two geometrical arrangements of defects. We calculated the binding energy of defect complex involving various lower energy point defects, and the result is summarized in Table 1, its chemical potential dependence is shown in Fig. 2.

The binding energy of defect complex can be negative because of the charge or stress compensation, and also Coulombic attraction between defects[55], thus it is expected that partial or fully compensated defect complexes may have a highly negative binding energy hence enhancing total de-

Table 1. Listing of absolute formation energy of defect complexes (meV) at chemical potential point B along with separated point defects; binding energy is independent of chemical potential.

Parameter	Cu_{Mg}+Mg_{Cu}		$(2Cu)_{Mg}$		$Mg_{(2Cu)}$		Mg_{Sn}+Sn_{Mg}		$(CuMg)_{Sn}$		$(CuMg)_{Sn}$		$(2Cu)_{Sn}$	
ΔH_α	Cu_{Mg}	0.44	Cu_{Mg}	0.44	V_{Cu}	1.29	Mg_{Sn}	1.89	Mg_i	3.75	Mg_{Sn}	1.89	Cu_{Sn}	2.28
ΔH_β	Mg_{Cu}	1.73	Cu_i	2.25	Mg_{Cu}	1.73	Sn_{Mg}	1.77	Cu_{Sn}	2.28	Cu_i	2.25	Cu_i	2.25
$\Delta H_{\alpha\beta}$	0.24		0.88		0.87		1.35		2.42		2.42		2.12	
E_{bind}	−1.93		−1.81		−2.15		−2.31		−3.61		−1.72		−2.41	

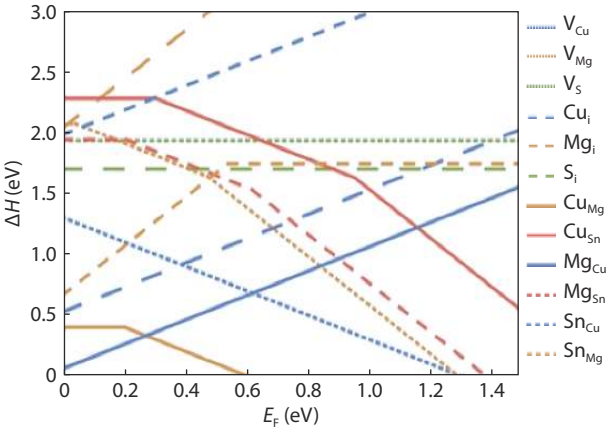

Fig. 3. (Color online) Charged defect formation energy of point defects at chemical potential B, Fermi energy is varied from VBM to CBM.

fect population.

Literature in CZTS showed that Cu–Zn disorder is partly responsible to V_{oc} loss, which may be explained by the low formation energy of Cu–Zn related defect complexes. In CMTS, we also show that fully compensated defect complexes Cu_{Mg}+Mg_{Cu}, $(2Cu)_{Mg}$ and $Mg_{(2Cu)}$ have a low formation energy less than 1 eV. The formation energy for Cu_{Mg}+Mg_{Cu} is 0.24 eV, similar to Cu_{Zn}+Zn_{Cu} in CZTS. Because of the low formation energy, the concentration of Cu_{Mg}+Mg_{Cu} at equilibrium can be as high as $>10^{20}$ cm^{-3}, which may not be desirable. Similarly to CZTS, these low energy defect complexes can possibly induce a Cu–Mg disorder phase in CMTS, and thus a careful control of growth temperature may also be required for the growth of CMTS.

Defect complexes involving Sn atom has a large binding energy due to stronger charge compensation between p- and n-type defects. In CZTS, Zn_{Sn}+Sn_{Zn} can induce strong band gap shrinking, which can be a significant contributor to band gap fluctuation because of its low formation energy of 0.86 eV[12].

The formation energy of Mg_{Sn}+Sn_{Mg} in CMTS is higher by +0.49 eV, possibly lowering its concentration by several orders of magnitude. For other defect complexes involving Sn, the absolute formation energy of Sn related defect complexes is not lowered significantly past that of an isolated point defect, together with the large binding energy. Such a mechanism may also help convert deep intrinsic defects into defect complexes that are less electrically active.

5. Electronic properties of defects

In this part, we examine the dependence of charge transition level on the Fermi energy level. The charged defect formation energy at chemical potential point B is shown in Fig. 3. In CMTS, Cu_{Mg} shows properties analogous to Cu_{Zn} in CZTS. Cu_{Mg} can be ionized to −1 charge state, the ionized state is energetically more favorable when Fermi energy level is higher than VBM + 0.21 eV, slightly deeper than Cu_{Zn} in CZTS[61]. Regardless of charge state, Cu_{Mg} is always the most favorable acceptor defect in CMTS, while V_{Cu}^- is at least 0.5 eV higher. We expect a slightly lower but comparable carrier concentration in CMTS, which is sufficient as a photovoltaic absorber. Mg_{Cu} and Cu_i are the dominant donor type defects in the CMTS system. However, both of them are ionized at all Fermi energy level within the band gap, and the formation energy of these ionized single donor defects are further lowered at VBM, at 0.10 and 0.65 eV, respectively, similar to CZTS. In general, the Fermi energy level pinning can be approximated by the Fermi energy level at which the formation energies of the lowest energy donor and acceptor are equal. We find this value in CMTS to be 0.27 eV by Cu_{Mg} and Mg_{Cu}, indicating that CMTS grown under Sn poor and Cu mildly poor condition is intrinsically p-type. However, at chemical potential point C, formation energy for donor defects are generally lower while higher for acceptor defects. At this growth condition, although Cu_{Mg} and Mg_{Cu} remain as the dominant p-type and n-type defects in the system, the Fermi energy pinning will shift to 0.6 eV, indicating possible lowering of p-type carrier concentration due to higher charge compensation, which may not be desirable.

Our calculations show that anion defects in CMTS do not show charge transition within the band gap. Acceptor defects Mg_{Sn} and Cu_{Sn} can have multiple transitions into lower energy negatively charged states as the Fermi energy level moves towards CBM. Around the pinned Fermi energy level, these defects remain charge neutral and has a high formation energy above 2 eV. However, we find that the Sn_{Mg} defect has a deep (0/2+) charge transition at VBM + 0.55 eV near the mid gap with relatively low formation energy of 1.77 eV in a neutral state at chemical potential point B, which can serve as carrier traps. Such a negative-U center is more detrimental than Sn_{Zn} in CZTS because of relatively low formation energy[61]. In turn, the control of the Sn_{Mg} defect is crucial to fabricate a CMTS photovoltaic device with high efficiency.

We then explore the scenario where defect concentration is high. At high defect concentration, defect bands may be formed leading to band tailing, which is commonly regarded as a major contribution to loss of open circuit voltage in CZTS[15]. We calculated the band edge shift for compensated defect complexes in CMTS and aligned with the host cell using core energy levels further away from the defect (Table 2). We find that antisite pairs, both Cu_{Mg}+Mg_{Cu} and Mg_{Sn}+Sn_{Mg}, may induce a sizable band tailing. For Cu_{Mg}+Mg_{Cu}, an upward shifting of VBM by 0.1 eV is found, while for Mg_{Sn}+Sn_{Mg}, a significant shrink of band gap by 0.45 eV is found, mainly attributed to the lowering of CBM. Controlling defect density of Mg_{Sn}+Sn_{Mg} is thus crucial to reduce possible band tailing in CMTS.

Table 2. Valence and conduction band edge shifts induced by low-energy fully compensated defect complexes in CMTS.

Parameter	ΔH at B (eV)	ΔVBM (meV)	ΔCBM (meV)	ΔE_g (meV)
$Cu_{Mg}+Mg_{Cu}$	0.24	+111	+12	−99
$(2Cu)_{Mg}$	0.88	+15	−13	−28
$Mg_{(2Cu)}$	0.87	−46	+57	103
$Mg_{Sn}+Sn_{Mg}$	1.35	+125	-325	−450
$(2Mg)_{Sn}$	1.95	+86	+72	−14

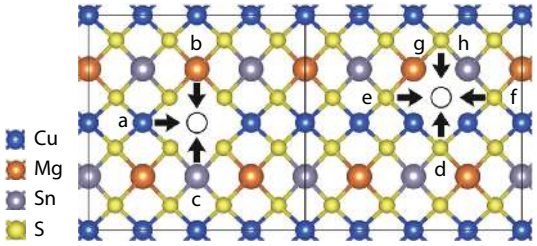

Fig. 4. (Color online) Illustration of vacancy diffusion paths investigated in the current study.

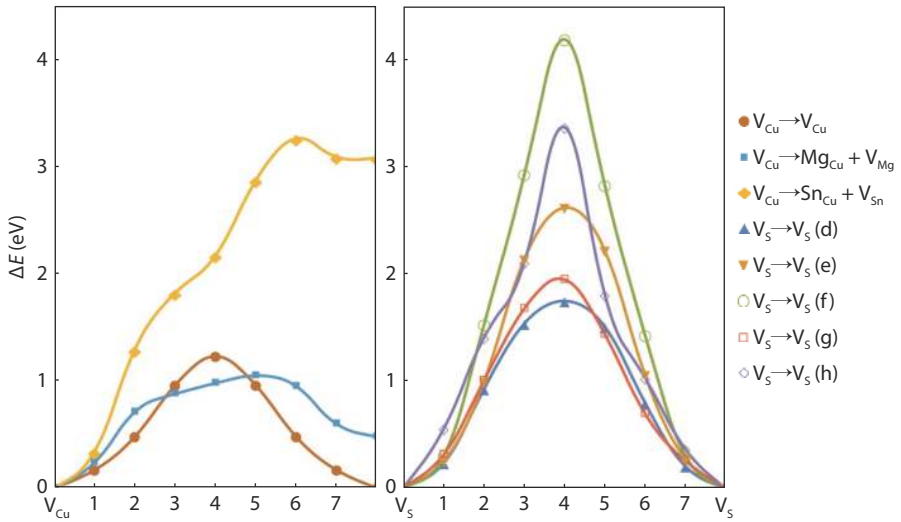

Fig. 5. (Color online) Energy relative to V_{Cu} for cation and V_S for anion diffusion along the MEP, energies of calculated images are represented by markers and solid lines are interpolation.

6. Vacancy-mediated diffusion

Lastly, we show our results regarding the diffusion kinetics of a few point defects in CMTS. Defect thermodynamics provide a good estimation of bulk defect density when spatial variation of atom stoichiometry can be minimized, that is, when the diffusion is relatively quick, it is thus important also to understand the diffusion kinetics in CMTS. As we have already showed that the formation energy of Cu and S vacancies are relatively low in CMTS, the density of these defects should be relatively high, thus our current result focuses on the diffusion of atoms in the presence of Cu or S vacancy. Moreover, the activation energy of diffusions through V_{Cu} is found to be relatively low in both CZTS and CIGS. Therefore, our result on CMTS can provide qualitative insight into the diffusion properties of CMTS. The chosen diffusion paths are shown in Fig. 4. Diffusion simulation is conducted via the nudged elastic band method with a climbing image using seven images between optimized initial and final defect configurations to provide smooth interpolation to the reaction energetics and good estimation of activation energy[62]. Due to much higher computational complexity of diffusion calculation, diffusion calculations are conducted using a Perdew–Burke–Ernzerhof (PBE) functional[63]. We checked our calculated activation energy to agree within 0.1 eV in CZTS and CIGS compared to previous literature values.

Relative energy along minimum energy path (MEP) is shown in Fig. 5. The activation energy for the diffusion of V_{Cu} is 1.23 eV in CMTS, which is similar to Cu diffusion via vacancies in CZTS and CIGS system. For Mg diffusion into V_{Cu}, the formation energy is 0.18 eV lower (1.05 eV). In comparison, Zn diffusion into V_{Cu} in CZTS is 0.13 eV higher than diffusion of copper vacancy, indicating that Mg is also a relatively mobile atom species in CMTS. On the other hand, Sn diffusion into V_{Cu} has a much higher activation energy. This is partly due to the higher formation energy of Sn defect and relatively large atomic size of Sn. This high diffusion barrier may also help to prevent the formation of Sn antisite defect, which we considered detrimental in CMTS. V_S represents the vacancy-mediated diffusion of S atom in CMTS with all initial and final configuration of V_S being equivalent, thus the energy profile along the MEP should be symmetric. Despite this, we have not enforced such symmetry during the calculation, and our result shows an almost symmetric energy profile, indicating that the images are well-converged to minimal energy. For all S vacancy diffusion in CMTS, the activation energy is at the minimal 1.86 eV with a strong asymmetry. When S atoms diffuse across Sn atoms, additional energy is required to lose the stronger S–Sn bonding, which results in the diffusion barrier of S across the Cu layer to be significantly lower. Our result shows calculated activation energy for Sn and S diffusion has an activation energy comparable to In diffusion in CISe[64], suggesting diffusion of Sn and S through our calculated MEP is difficult. It should be noted that S or Sn diffusion can be facilitated by the presence of grain boundaries or off-stoichiometry conditions, which are not modelled by the current calculation.

7. Conclusion

We presented a systematic study of point defects and a

few defect complexes in CMTS using the HSE06 functional within the density functional theory framework. Our calculation shows that the growth window of CMTS is similar to that of CZTS, and there is an increase in formation energy for most defects compared to CZTS hence a lower defect density. Such an elevation reduces the concentration of Mg_{Sn} and Cu_{Sn} defects with multiple charge states. Then we predict a p-type behavior due to ionization of Cu_{Mg} to Cu_{Mg}^{-}, showing the Fermi energy located around 0.2 eV above the valence band due to compensation with a Mg_{Cu} defect. However, we still unearth a strong Cu/Mg compositional fluctuation due to low formation energy for a Cu_{Mg}+Mg_{Cu} defect complex, analogous to CZTS results. And we identify Sn_{Mg} double donor defect as the likely detrimental defect in CMTS system because of high density at Sn-rich or Cu-rich chemical potential, and a deep donor level in the mid gap. The profile of the Sn_{Mg} defect is inferior than Sn_{Zn} in CZTS. To avoid a high concentration of the Sn_{Mg} defect, we propose tuning the chemical potential to Sn-poor and Cu mildly poor condition or anneal at lower temperature. Finally, we justify our defect finding with a comparison of activation energy of vacancy diffusion in CMTS and CZTS. We find the Cu and Mg diffusion through V_{Cu} to be relatively quick, and the activation energy of these diffusion mechanisms are similar to previous reported values in CZTS and CIGS.

Acknowledgements

The authors would like to acknowledge support from Research Grants Council of Hong Kong (under GRF/14319416, GRF/14301318, and Direct Grant).

References

[1] Chen S Y, Gong X G, Walsh A, et al. Crystal and electronic band structure of Cu_2ZnSnX_4 (X = S and Se) photovoltaic absorbers: First-principles insights. Appl Phys Lett, 2009, 94, 041903

[2] He J, Sun L, Chen S Y, et al. Composition dependence of structure and optical properties of $Cu_2ZnSn(S, Se)_4$ solid solutions: An experimental study. J Alloys Compd, 2012, 511, 129

[3] Levcenco S, Dumcenco D, Wang Y P, et al. Influence of anionic substitution on the electrolyte electroreflectance study of band edge transitions in single crystal $Cu_2ZnSn(S_xSe_{1-x})_4$ solid solutions. Opt Mater, 2012, 34, 1362

[4] Persson C. Electronic and optical properties of Cu_2ZnSnS_4 and $Cu_2ZnSnSe_4$. J Appl Phys, 2010, 107, 053710

[5] Wang W, Winkler M T, Gunawan O, et al. Device characteristics of CZTSSe thin-film solar cells with 12.6% efficiency. Adv Energy Mater, 2014, 4, 1301465

[6] Yan C, Huang J L, Sun K W, et al. Cu_2ZnSnS_4 solar cells with over 10% power conversion efficiency enabled by heterojunction heat treatment. Nat Energy, 2018, 3, 764

[7] Liu X L, Feng Y, Cui H T, et al. The current status and future prospects of kesterite solar cells: A brief review. Prog Photovolt: Res Appl, 2016, 24, 879

[8] Bishop D M, McCandless B, Gershon T, et al. Modification of defects and potential fluctuations in slow-cooled and quenched $Cu_2ZnSnSe_4$ single crystals. J Appl Phys, 2017, 121, 065704

[9] Zhuk S, Kushwaha A, Wong T K S, et al. Critical review on sputter-deposited Cu_2ZnSnS_4 (CZTS) based thin film photovoltaic technology focusing on device architecture and absorber quality on the solar cells performance. Sol Energy Mater Sol Cells, 2017, 171, 239

[10] Gunawan O, Todorov T K, Mitzi D B. Loss mechanisms in hydrazine-processed $Cu_2ZnSn(Se, S)_4$ solar cells. Appl Phys Lett, 2010, 97, 233506

[11] Han D, Sun Y Y, Bang J, et al. Deep electron traps and origin of p-type conductivity in the earth-abundant solar-cell material Cu_2ZnSnS_4. Phys Rev B, 2013, 87, 155206

[12] Chen S Y, Walsh A, Gong X G, et al. Classification of lattice defects in the kesterite Cu_2ZnSnS_4 and $Cu_2ZnSnSe_4$ earth-abundant solar cell absorbers. Adv Mater, 2013, 25, 1522

[13] Gokmen T, Gunawan O, Todorov T K, et al. Band tailing and efficiency limitation in kesterite solar cells. Appl Phys Lett, 2013, 103, 103506

[14] Romero M J, Du H, Teeter G, et al. Comparative study of the luminescence and intrinsic point defects in the kesterite Cu_2ZnSnS_4 and chalcopyrite $Cu(In, Ga)Se_2$ thin films used in photovoltaic applications. Phys Rev B, 2011, 84, 165324

[15] Rey G, Larramona G, Bourdais S, et al. On the origin of band-tails in kesterite. Sol Energy Mater Sol Cells, 2018, 179, 142

[16] Li J J, Wang D X, Li X L, et al. Cation substitution in earth-abundant kesterite photovoltaic materials. Adv Sci, 2018, 5, 1700744

[17] Pal K, Singh P, Bhaduri A, et al. Current challenges and future prospects for a highly efficient (>20%) kesterite CZTS solar cell: A review. Sol Energy Mater Sol Cells, 2019, 196, 138

[18] Kanevce A, Repins I, Wei S H. Impact of bulk properties and local secondary phases on the $Cu_2(Zn, Sn)Se_4$ solar cells open-circuit voltage. Sol Energy Mater Sol Cells, 2015, 133, 119

[19] Kosyak V, Postnikov A V, Scragg J, et al. Calculation of point defect concentration in Cu_2ZnSnS_4: Insights into the high-temperature equilibrium and quenching. J Appl Phys, 2017, 122, 035707

[20] Huang D, Persson C. Band gap change induced by defect complexes in Cu_2ZnSnS_4. Thin Solid Films, 2013, 535, 265

[21] Zawadzki P, Zakutayev A, Lany S. Entropy-driven clustering in tetrahedrally bonded multinary materials. Phys Rev Appl, 2015, 3, 034007

[22] Scragg J J S, Choubrac L, Lafond A, et al. A low-temperature order-disorder transition in Cu_2ZnSnS_4 thin films. Appl Phys Lett, 2014, 104, 041911

[23] Mendis B G, Goodman M C J, Major J D, et al. The role of secondary phase precipitation on grain boundary electrical activity in Cu_2ZnSnS_4 (CZTS) photovoltaic absorber layer material. J Appl Phys, 2012, 112, 124508

[24] Yang W C, Miskin C K, Carter N J, et al. Compositional inhomogeneity of multinary semiconductor nanoparticles: A case study of Cu_2ZnSnS_4. Chem Mater, 2014, 26, 6955

[25] Scragg J J, Wätjen J T, Edoff M, et al. A detrimental reaction at the molybdenum back contact in $Cu_2ZnSn(S, Se)_4$ thin-film solar cells. J Am Chem Soc, 2012, 134, 19330

[26] Scragg J J, Kubart T, Wätjen J T, et al. Effects of back contact instability on Cu_2ZnSnS_4 devices and processes. Chem Mater, 2013, 25, 3162

[27] Dalapati G K, Zhuk S, Masudy-Panah S, et al. Impact of molybdenum out diffusion and interface quality on the performance of sputter grown CZTS based solar cells. Sci Rep, 2017, 7, 1350

[28] Bär M, Schubert B A, Marsen B, et al. Cliff-like conduction band offset and KCN^--induced recombination barrier enhancement at the CdS/Cu_2ZnSnS_4 thin-film solar cell heterojunction. Appl Phys Lett, 2011, 99, 222105

[29] Nagaoka A, Miyake H, Taniyama T, et al. Effects of sodium on electrical properties in Cu_2ZnSnS_4 single crystal. Appl Phys Lett, 2014, 104, 152101

[30] Gershon T, Shin B, Bojarczuk N, et al. The role of sodium as a surfactant and suppressor of non-radiative recombination at internal surfaces in Cu_2ZnSnS_4. Adv Energy Mater, 2015, 5, 1400849

[31] Zhang Y O, Tse K, Xiao X D, et al. Controlling defects and secondary phases of CZTS by surfactant potassium. Phys Rev Mater, 2017, 1, 045403

[32] Yan C, Liu F Y, Song N, et al. Band alignments of different buffer lay-

ers (CdS, Zn(O, S), and In_2S_3) on Cu_2ZnSnS_4. Appl Phys Lett, 2014, 104, 173901
[33] Sun K W, Yan C, Liu F Y, et al. Over 9% efficient kesterite Cu_2ZnSnS_4 solar cell fabricated by using $Zn_{1-x}Cd_xS$ buffer layer. Adv Energy Mater, 2016, 6, 1600046
[34] Li X L, Su Z H, Venkataraj S, et al. 8.6% Efficiency CZTSSe solar cell with atomic layer deposited Zn-Sn-O buffer layer. Sol Energy Mater Sol Cells, 2016, 157, 101
[35] Li J J, Liu X R, Liu W, et al. Restraining the band fluctuation of CBD-Zn(O, S) layer: Modifying the hetero-junction interface for high performance $Cu_2ZnSnSe_4$ solar cells with Cd-free buffer layer. Sol RRL, 2017, 1, 1700075
[36] Cui H T, Liu X L, Liu F Y, et al. Boosting Cu_2ZnSnS_4 solar cells efficiency by a thin Ag intermediate layer between absorber and back contact. Appl Phys Lett, 2014, 104, 041115
[37] Liu F Y, Sun K W, Li W, et al. Enhancing the Cu_2ZnSnS_4 solar cell efficiency by back contact modification: Inserting a thin TiB_2 intermediate layer at Cu_2ZnSnS_4/Mo interface. Appl Phys Lett, 2014, 104, 051105
[38] Liu X L, Cui H T, Li W, et al. Improving Cu_2ZnSnS_4 (CZTS) solar cell performance by an ultrathin ZnO intermediate layer between CZTS absorber and Mo back contact. Phys Status Solidi RRL, 2014, 8, 966
[39] Tong Z F, Zhang K, Sun K W, et al. Modification of absorber quality and Mo-back contact by a thin Bi intermediate layer for kesterite Cu_2ZnSnS_4 solar cells. Sol Energy Mater Sol Cells, 2016, 144, 537
[40] Gu Y C, Shen H P, Ye C, et al. All-solution-processed Cu_2ZnSnS_4 solar cells with self-depleted Na_2S back contact modification layer. Adv Funct Mater, 2018, 28, 1703369
[41] Wang C C, Chen S Y, Yang J H, et al. Design of I2–II–IV–VI_4 semiconductors through element substitution: The thermodynamic stability limit and chemical trend. Chem Mater, 2014, 26, 3411
[42] Zhong G H, Tse K, Zhang Y O, et al. Induced effects by the substitution of Zn in Cu_2ZnSnX_4 (X = S and Se). Thin Solid Films, 2016, 603, 224
[43] Yuan Z K, Chen S Y, Xiang H J, et al. Engineering solar cell absorbers by exploring the band alignment and defect disparity: The case of Cu- and Ag-based kesterite compounds. Adv Funct Mater, 2015, 25, 6733
[44] Qi Y F, Kou D X, Zhou W H, et al. Engineering of interface band bending and defects elimination via a Ag-graded active layer for efficient $(Cu, Ag)_2ZnSn(S, Se)_4$ solar cells. Energy Environ Sci, 2017, 10, 2401
[45] Su Z H, Tan J M R, Li X L, et al. Cation substitution of solution-processed Cu_2ZnSnS_4 thin film solar cell with over 9% efficiency. Adv Energy Mater, 2015, 5, 1500682
[46] Bag S, Gunawan O, Gokmen T, et al. Hydrazine-processed Ge-substituted CZTSe solar cells. Chem Mater, 2012, 24, 4588
[47] Collord A D, Hillhouse H W. Germanium alloyed kesterite solar cells with low voltage deficits. Chem Mater, 2016, 28, 2067
[48] Wei M, Du Q Y, Wang R, et al. Synthesis of new earth-abundant kesterite Cu_2MgSnS_4 nanoparticles by hot-injection method. Chem Lett, 2014, 43, 1149
[49] Agawane G L, Vanalakar S A, Kamble A S, et al. Fabrication of $Cu_2(Zn_xMg_{1-x})SnS_4$ thin films by pulsed laser deposition technique for solar cell applications. Mater Sci Semicond Process, 2018, 76, 50
[50] Yang G, Zhai X L, Li Y F, et al. Synthesis and characterizations of Cu_2MgSnS_4 thin films with different sulfuration temperatures. Mater Lett, 2019, 242, 58
[51] Caballero R, Haass S G, Andres C, et al. Effect of magnesium incorporation on solution-processed kesterite solar cells. Front Chem, 2018, 6, 5
[52] Lie S, Leow S W, Bishop D M, et al. Improving carrier-transport properties of CZTS by Mg incorporation with spray pyrolysis. ACS Appl Mater Interfaces, 2019, 11, 25824
[53] Chen S Y, Yang J H, Gong X G, et al. Intrinsic point defects and complexes in the quaternary kesterite semiconductor Cu_2ZnSnS_4. Phys Rev B, 2010, 81, 245204
[54] Hinuma Y, Grüneis A, Kresse G, et al. Band alignment of semiconductors from density-functional theory and many-body perturbation theory. Phys Rev B, 2014, 90, 155405
[55] Wei S H. Overcoming the doping bottleneck in semiconductors. Comput Mater Sci, 2004, 30, 337
[56] Freysoldt C, Neugebauer J, van de Walle C G. Fully ab initio finite-size corrections for charged-defect supercell calculations. Phys Rev Lett, 2009, 102, 016402
[57] Chen S Y, Gong X G, Walsh A, et al. Electronic structure and stability of quaternary chalcogenide semiconductors derived from cation cross-substitution of II-VI and I-III-VI2 compounds. Phys Rev B, 2009, 79, 165211
[58] Zhu J Y, Liu F, Stringfellow G B, et al. Strain-enhanced doping in semiconductors: Effects of dopant size and charge state. Phys Rev Lett, 2010, 105, 195503
[59] Hu H, Liu M, Wang Z F, et al. Quantum electronic stress: Density-functional-theory formulation and physical manifestation. Phys Rev Lett, 2012, 109, 055501
[60] Noufi R, Axton R, Herrington C, et al. Electronic properties versus composition of thin films of $CuInSe_2$. Appl Phys Lett, 1984, 45, 668
[61] Xiao W, Wang J N, Zhao X S, et al. Intrinsic defects and Na doping in Cu_2ZnSnS_4: A density-functional theory study. Sol Energy, 2015, 116, 125
[62] Henkelman G, Uberuaga B P, Jónsson H. A climbing image nudged elastic band method for finding saddle points and minimum energy paths. J Chem Phys, 2000, 113, 9901
[63] Perdew J P, Burke K, Ernzerhof M. Generalized gradient approximation made simple. Phys Rev Lett, 1996, 77, 3865
[64] Nakamura S, Maeda T, Wada T. First-principles study of diffusion of Cu and in atoms in $CuInSe_2$. Jpn J Appl Phys, 2013, 52, 04CR01

Kin Fai Tse has obtained his Ph.D. and Bsc degrees in Physics at The Chinese University of Hong Kong in 2020 and 2015, respectively. His research interest is focus on defects in photovoltaic materials.

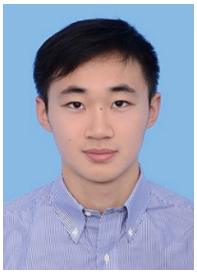

Shengyuan Wang is currently a Ph.D. student in Department of Physics at The Chinese University of Hong Kong. He has obtained his Bachelor's degree in Physics at Shanghai Jiao Tong University in 2020. His research interest is focus on defect and surface calculations in the area of semiconductor physics.

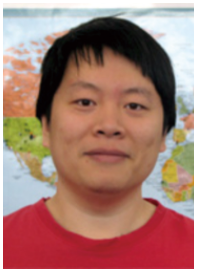

Junyi Zhu is an associate professor at the Department of Physics, The Chinese University of Hong Kong. He received his B.S. degree from Peking University in 1998. He received his Ph.D. degree from University of Utah in 2009. His research interests mainly include semiconductor defects and doping, electronic properties of solids, surface and interface phenomena, using first-principles and molecular dynamics approaches and elastic theory modeling.